Dynamics of field-driven population inversion in a confined colloidal mixture

S. Chung,[1] S. Samin,[2] C. Holm,[3] J. G. Malherbe,[1] and S. Amokrane[1,*]

[1]*Physique des Liquides et Milieux Complexes, Faculté des Sciences et Technologie, Université Paris–Est (Créteil), 61 Avenue du Général de Gaulle, 94010 Créteil Cedex, France*

[2]*Center for Extreme Matter and Emergent Phenomena, Institute for Theoretical Physics, Utrecht University, Princetonplein 5, 3584 CC Utrecht, The Netherlands*

[3]*Institute for Computational Physics, Universität Stuttgart, Allmandring 3, 70569 Stuttgart Germany*

(Received 29 November 2016; published 13 February 2017)

We study, using Langevin dynamics simulations, the change in composition of a binary colloidal mixture confined in a finite-length channel, induced by an external field. The field-induced transition from a near-bulk composition to an inverted population is studied as a function of time, for different field strengths and system parameters. For state points corresponding to reversible field cycles, the cyclic filling and emptying of the channel by the minority species are compared. Extrapolation of the physical relaxation times to the colloidal regime is performed through a series of simulations at increasing value of the damping parameter. For state points at which the mixture is unstable at zero field, reproducible irreversible cycles are illustrated. For reversible field cycles, the scaling with the particles size of the characteristic cycling time is discussed.

DOI: 10.1103/PhysRevE.95.022605

I. INTRODUCTION

Due to their importance in domains ranging from materials science to biology, fluids confined in external fields have been the subject of continued interest. While molecular fluids have been studied extensively [1–3], emphasis has recently been put on confined colloids, due to the possibility to tune the effective interaction between macroparticles and their phase behavior by various fields. Besides specific factors such as composition, geometry, and interaction strength, electric (magnetic) fields indeed affect the static and dynamic behavior of confined fluids by exerting forces or torques on the dipolar particles, thus lowering their potential energy. Understanding the dynamical behavior of the fluid is of great importance in many applications, in which the fundamental mechanism relies on the difference between consecutive states of the systems. This gave rise to intense experimental and theoretical work on the equilibrium and dynamical field effects on confined fluids [4–23].

Among the studies dealing with the control of confined fluids by external fields, Brunet *et al.* [8,9] discussed the potentially useful phenomenon of a field-induced population inversion near bulk instability of binary mixtures (PINBI). The authors of Refs. [8,9] showed that, under certain conditions, it is possible to produce a field-induced jump in the adsorption of the confined minority component. Without repeating the arguments detailed in the original articles, we recall here that the field-induced PINBI effect results [8] from the combination of two actually quite generic physical mechanisms: (1) the effect of an electric field on polar particles and (2) large composition fluctuations in an open pore when the bulk mixture is close to a phase transition. Furthermore, the required ingredients, polar or polarizable particles and mixtures with unfavorable AB interactions, are quite common. Reference [9] also stressed the fact that a field control of the composition of the confined fluid that does not rely on a subtle combination of specific interactions should be robust and feasible with simple components. In experimental realizations, chemical specificity would enter through the composition of the stabilizing layers of the colloids, so as to facilitate the demixing.

The authors suggested that the resulting discontinuity in the physical properties of the mixture could be used for a range of possible applications, for example, to modulate the dielectric response of a confined fluid for optical applications or its viscosity for electromechanical ones. A similar population change in other confined binary mixtures, driven by density or specific interactions, has been discussed in Refs. [10–13]. The idea of considering a system made of a bulk region and a finite region of space, in which the external potentials are applied to achieve local changes, is also present in other studies. For instance, size selectivity in ion channels through an effective potential is considered in Ref. [24] and density or composition modulation by local external potentials in Ref. [25], besides the studies of Refs. [10–13]. We stress that the field effect discussed here (and also with the optical tweezers technique suggested in [25]) is obtained without affecting the state or the bulk fluid or having to tune its composition. This is an important advantage in comparison with other methods in which selectivity requires a permanent specific field that cannot be changed simply.

Up to now, the studies of PINBI have been concerned with the equilibrium structure and static properties, including the intriguing interplay of the population change with the phase and structural transitions [26,27]; see also Ref. [28] for a similar study on confined dipolar fluids. A natural next step is to investigate the dynamical nonequilibrium aspects of the population inversion. Questions such as how long it takes for the population to be inverted by the external field (filling by the minority species), what happens when the field is subsequently turned off, and what the characteristic filling time is and how it is affected by the system parameters are all significant for the realization of applications that rely on the time evolution or, conversely, the fast response of the density and composition of the confined fluid. In this paper we give at least qualitative answers to some of these questions.

*Corresponding author: amokrane@u-pec.fr

TABLE I. Parameters of the WCA potential giving the same second virial coefficients $B_{ij}^{(2)}$ as those of hard-sphere mixtures.

		1-2 interaction	
Parameters	1-1–2-2 interaction	Nearly additive	Nonadditive
$\sigma_{ij}^{\mathrm{HS}}/\sigma_{\mathrm{HS}}$	1	1.01624	1.2
$B_{ij}^{(2)}/\sigma_{\mathrm{HS}}^3$	2.09	2.20	3.62
WCA	$(\lambda = 0.9, \epsilon^* = 1)$	$(\lambda = 0.92, \epsilon^* = 0.37)$	$(\lambda = 1.08, \epsilon^* = 1)$

We start from the same basic situation considered in previous studies [8,9], that of a geometrically confined binary mixture in which one species is dipolar and thus benefits from an interaction with an external field. We consider states points in the phase diagram close to the bulk demixing, so as to make the external field effect more pronounced. The relaxation towards equilibrium depends on the specific geometry. We consider confinement in a finite-size slitlike channel in contact with a bulk mixture through a true interfacial region. This situation is closer to experimental realizations such as in microfluidic devices than the infinite open pore usually considered in similar studies. We conducted extensive Langevin dynamics simulations, focusing, among the relevant physical parameters, on the influence of the field strength on the channel filling and emptying. We also present results for increasing values of the implicit solvent friction parameters, which we then use to extrapolate the physical relaxation times to the colloidal regime.

This paper is organized as follows. In Sec. II we present the model and the simulation technique. In Sec. III results for the dynamics of the composition change are given. The main results are summarized in Sec. IV

II. MODEL AND SIMULATION TECHNIQUES

A. Model

We consider a binary mixture of uncharged spheres (labeled 1) and dipolar ones (labeled 2) of equal effective hard-sphere diameter σ_{HS}. We aim at modeling a mixture of hard-sphere-like colloidal system with a large difference in the dipole moment; see, for example, Refs. [5,29,30] for recent experimental work. To avoid the difficulties with discontinuous potentials in molecular dynamics (MD) simulation, the hard-sphere part of the pairwise interaction is replaced by a softer, purely repulsive, Lennard-Jones potential treated in the Weeks-Chandler-Andersen (WCA) fashion [31]:

$$u_{ij}(r) = \begin{cases} 4\epsilon_{ij}\left[\left(\frac{\sigma_{ij}}{r}\right)^{12} - \left(\frac{\sigma_{ij}}{r}\right)^{6}\right] + \epsilon_{ij} & \text{if } r \leqslant 2^{1/6}\sigma_{ij} \\ 0 & \text{otherwise.} \end{cases} \quad (1)$$

For simplicity, we take the same interaction potential between like spheres, all particles with the walls, but a different one between unlike spheres, since this is one important ingredient of the PINBI effect. We choose to specify the diameters σ_{ij} and use the interaction strengths ϵ_{ij} to match the hard-sphere interaction through the virial equivalence. The plain WCA potential is however rather soft, its range of the order of $0.1\sigma_{ij}$ being too large for modeling hard-sphere-like colloids. Therefore, we take $\sigma_{ij} = \lambda_{ij}\sigma_{\mathrm{HS}}$ with $\lambda_{ij} < 1$ to have a steeper variation of $u_{ij}(r)$ at the scale of σ_{HS} (see Table I). Hereafter, σ_{HS} will be used as the unit of length; its value will depend on the specific system that is considered. A typical value for colloids is $\sigma_{\mathrm{HS}} \approx 1\ \mu$m. To set the interaction strength in the range corresponding to colloids, we took $\lambda_{11} = \lambda_{22} = 0.9$. The common interaction strength $\epsilon_{11}/k_{\mathrm{B}}T = \epsilon_{22}/k_{\mathrm{B}}T$, with T the temperature and k_{B} the Boltzmann constant, is determined from the second virial coefficient $B^{(2)}$ by setting the $B_{\mathrm{WCA}}^{(2)} = B_{\mathrm{HS}}^{(2)}$ and the relation $B_{\mathrm{HS}}^{(2)} = 2\pi\sigma_{\mathrm{HS}}^3/3$ for hard spheres. The $\epsilon_{ii}/k_{\mathrm{B}}T$ determined in this manner is independent of σ_{HS}, since the WCA potential depends only on the reduced distance r/σ. It does however depend on λ_{ii}, giving $\epsilon_{11}/k_{\mathrm{B}}T = 194$ for $\lambda_{11} = 0.9$. In Sec. III B 3, in which we discuss the size dependence of the interaction strength, we show that the energy scale $e_0 = 194k_{\mathrm{B}}T_a \approx 8 \times 10^{-19}$ J, with $T_a = 300$ K the ambient temperature, sets an appropriate scale for the strength of the *repulsive* potential between hard-sphere-like colloidal particles. The typical value of $\epsilon/k_{\mathrm{B}}T \sim 1$ appropriate to the molecular scale would be obtained with λ closer to unity; for example, $\lambda = 0.98$ gives $\epsilon/k_{\mathrm{B}}T = 1.034$. Hereafter, we will use for convenience e_0 as the energy scale.

By taking different values for the cross diameter σ_{12}, it is possible to simulate a positive nonadditivity that destabilizes the mixture [32,33] and favors population inversion at low fields [9]. The nonadditivity is matched to that of a hard-spheres mixture, in which the cross diameter is $\sigma_{ij}^{\mathrm{HS}} = \frac{1}{2}(\sigma_i^{\mathrm{HS}} + \sigma_j^{\mathrm{HS}})(1+\delta)$, with a positive nonadditivity δ, through the second virial coefficient $B_{12}^{(2)}$. We use ϵ_{12} as the fitting parameter, while σ_{12} is fixed to $\lambda\sigma_{12}^{\mathrm{HS}}$ (chosen so as to have ϵ_{12} not too different from e_0). Two models are considered: (i) a nearly additive mixture with $\delta = 0.016$ and (ii) a nonadditive mixture with $\delta = 0.2$. The corresponding values of $\epsilon^* = \epsilon_{ij}/e_0$, $\lambda_{ij} = \sigma_{ij}/\sigma_{\mathrm{HS}}$, and $B_{ij}^{(2)}$ are given in Table I and interaction potentials are plotted in Fig. 1.

The dipolar hard spheres carry a point dipole $\boldsymbol{\mu}$ at their center. To avoid the complication of having to determine the self-consistent local field during the simulation (see [34] and references therein), we assume that the dipole is permanent. The dipoles interact through the dipolar potential

$$u_{\mathrm{dip}}^{ij} = \frac{1}{4\pi\varepsilon_{\mathrm{eff}}}\left[\frac{\boldsymbol{\mu}_i \cdot \boldsymbol{\mu}_j}{r_{ij}^3} - 3\frac{(\boldsymbol{\mu}_i \cdot \boldsymbol{r}_{ij})(\boldsymbol{\mu}_j \cdot \boldsymbol{r}_{ij})}{r_{ij}^5}\right], \quad (2)$$

where $\varepsilon_{\mathrm{eff}} = \varepsilon_{\mathrm{r}}\varepsilon_0$ is the effective dielectric constant of the confined fluid with ε_0 the permittivity of the vacuum. For convenience, we express the dipole moment as $\mu = \mu^*\sqrt{e_0\varepsilon_0\sigma_{\mathrm{HS}}^3}$. In the simulations, we use a dimensionless value $\mu^* = 0.49$, corresponding to $\mu = 1.3 \times 10^{-24}$ Cm with $\sigma_{\mathrm{HS}} = 1\ \mu$m and $e_0 = 194k_{\mathrm{B}}T_{\mathrm{a}}$, and a relative permittivity $\varepsilon_{\mathrm{r}} = 10$. This relatively low value is consistent with the absence of free

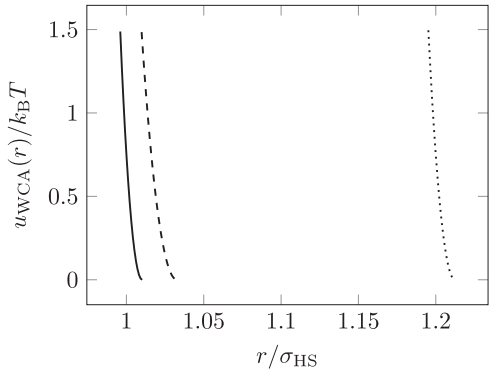

FIG. 1. Plot of the WCA potentials for the 1-1 and 2-2 interactions (solid line) and the nearly additive (dashed line) and nonadditive (dotted line) mixtures (1-2 interaction).

charges in the model [9]. The confinement geometry is shown in Fig. 2. The confined fluid exchanges particles with the surrounding bulk through an interface formed with rounded WCA walls [a quarter of circle in the (x,z) plane], thus forming a bottlenecklike channel; the system is assumed to be infinite in the y direction. The extent in the x direction of the bulk part is twice the channel length, to reduce the length of the simulations. This geometry corresponds, in fact, to a network of channels interconnected by bulklike regions, but this should not create qualitative differences from the situation of a single channel. Note that this particular geometry is chosen so as to facilitate the study by molecular dynamics of a finite pore with an explicit and smooth interface with the bulk. The symmetry is imposed to enable the use of periodic boundary conditions, in particular in the treatment of the electrostatics with existing three-dimensional algorithms (see below).

The distance between the WCA walls is taken in most cases to be $H^{\mathrm{slit}} = 7\sigma_{\mathrm{HS}}$, in order to reduce the jamming effect at higher confinement that significantly hinders particle motion and hence slows down the composition changes. A nonuniform external electric field $\boldsymbol{E}(x,z)$ is applied in the channel, with a direction normal to the walls in the central region. It is the sum of the electric fields created by two oppositely charged plates: $\boldsymbol{E}(x,z) = \boldsymbol{E}_+(x,z+(H^{\mathrm{slit}}+\sigma_{\mathrm{HS}})/2) + \boldsymbol{E}_-(x,z-(H^{\mathrm{slit}}+\sigma_{\mathrm{HS}})/2)$. The plates of extent $a = 10\sigma_{\mathrm{HS}}$ in the x direction bear a surface charge density $\pm q$.

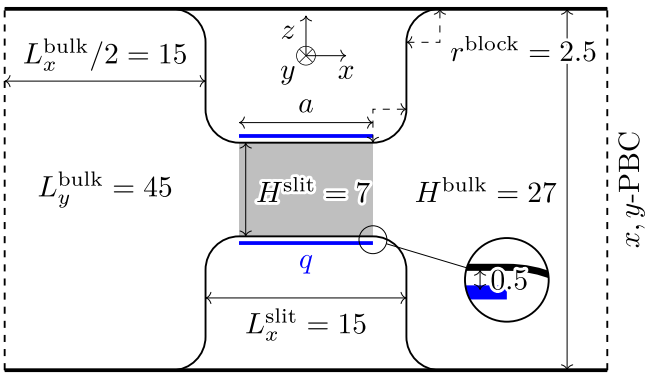

FIG. 2. Slit pore geometry used in the simulations. Lengths are in units of σ_{HS}.

The field generated in a medium with effective permittivity $\varepsilon_{\mathrm{eff}}$ is given by

$$\boldsymbol{E}_{\pm}(x,z) = \frac{\pm q}{4\pi\varepsilon_{\mathrm{eff}}}\boldsymbol{b}(x,z), \tag{3}$$

with

$$b_x(x,z) = \ln\left[\frac{(x+a/2)^2+z^2}{(x-a/2)^2+z^2}\right], \tag{4}$$

$$b_y(x,z) = 0, \tag{5}$$

$$b_z(x,z) = 2\left[\arctan\left(\frac{x+a/2}{z}\right) - \arctan\left(\frac{x-a/2}{z}\right)\right]. \tag{6}$$

In our simulation, we use the reduced surface charge density $q^* = q/\sqrt{e_0\varepsilon_0/\sigma_{\mathrm{HS}}^3}$. For $\varepsilon_{\mathrm{r}} = 10$, a field of $E = 2.5\times 10^5$ V/m in the center of the channel is obtained by setting $q^* = 14.3$.

The finite plates have an offset of $\sigma_{\mathrm{HS}}/2$ from the WCA walls (cf. Fig. 2), in order to minimize the effect of image forces, assuming continuity of the dielectric constant throughout the system. To achieve these conditions in practice, $\varepsilon_{\mathrm{eff}}$ should thus be close to the permittivity of the walls. As we do not aim at being quantitative, we also assume that the plates are uniformly charged, in spite of being of finite width. As shown in Fig. 3, the field is not completely negligible in the bulk, but its strength is much smaller than in the channel.

To summarize, the reduced input parameters in the MD simulations are $\sigma_{ij}/\sigma_{\mathrm{HS}}$ and ϵ_{ij}/e_0 for the WCA potential and q^*, μ^*, and ε_{r} for the applied field and the dipolar potential, and the reduced temperature $T^* = k_{\mathrm{B}}T/e_0$. Finally, a reduced friction coefficient γ^* also needs to be set, since the temporal evolution of the particles is governed by the Langevin dynamics equation, given here for the translational degrees of freedom for particle i as

$$m\ddot{\boldsymbol{r}}_i = -\boldsymbol{\nabla}_i U_i - \gamma\dot{\boldsymbol{r}}_i + \boldsymbol{W}_i(t), \tag{7}$$

where U_i is the total potential energy of the ith particle, γ is the friction coefficient, and $\boldsymbol{W}_i$ is the random force on particle i, related to γ such that the fluctuation-dissipation theorem is obeyed.

From the particle's mass m and friction coefficient γ, one defines a characteristic relaxation time $\tau_{\mathrm{R}} = m/\gamma$. Conversely,

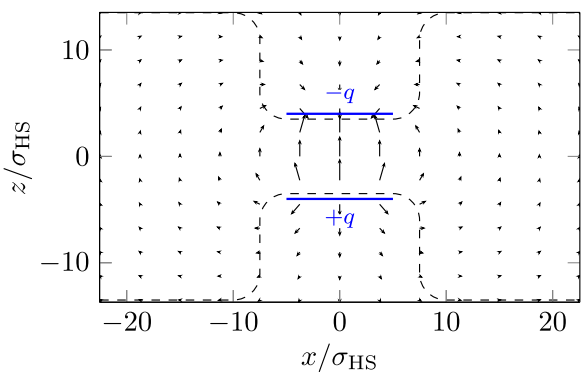

FIG. 3. Distribution of the applied field across the system. The arrow length is proportional to the field strength.

a thermostat-independent time unit τ_N (or Newtonian time unit) can be defined from the interaction potential. For the WCA potential

$$\tau_N = \sigma_{HS}\sqrt{m/e_0}, \tag{8}$$

from which a reduced friction coefficient is defined as $\gamma^* = \gamma\tau_N/m = \tau_N/\tau_R$. Numerical values of γ can be estimated from the Stokes-Einstein relation for a sphere of diameter σ in a solvent with viscosity η_s as $\gamma = 3\pi\sigma\eta_s$. Using $m = \rho_{water}\pi\sigma_{HS}^3/6$ with $\sigma_{HS} = 1$ μm gives $m = 5.23 \times 10^{-16}$ kg. The resulting time scale is $\tau_N = 2.55 \times 10^{-5}$ s, and using for the viscosity $\eta_s = 10^{-3}$ Pa s one obtains $\gamma = 9.42 \times 10^{-9}$ kg/s, corresponding to a reduced friction coefficient $\gamma^* = 460$. For such a large value of γ^* the simulation time would then be prohibitive. Therefore, we choose to perform a series of runs at increasing (but much smaller) values of γ^*. This choice sets the time scale for the dynamics and we find it instructive to plot the time evolution of relevant quantities is seconds, assuming the typical value of the physical parameters. However, caution is required before interpreting this as the evolution in real time, for the reasons detailed in Sec. III B 3.

Another issue is the choice of an appropriate ensemble. To simulate an infinite bulk reservoir at fixed chemical potentials, one should work in a grand canonical ensemble. However, we found that the canonical (N, V, and T) conditions are more suited to the geometry used here, aimed at obtaining absolute values of the relaxation times for a finite reservoir. Since some particles need in effect to travel from the outermost part of the bulklike region to the channel, this makes the relaxation times for composition changes dependent on the specific geometry. On the other hand, for an infinitely large reservoir, one would have to simulate very large systems in order to obtain relaxation times that do not depend on the extent of the reservoirs. Therefore, we use N_1, N_2, V, and T as the control variables, particle numbers, total volume, and temperature also being accessible experimentally.

To achieve a state point in the bulk that remains outside the two-phase domain in the simulation box we use results from previous work [8,9] for the hard-sphere mixture, to which the steep WCA potentials should be relevant. The simulation box is filled with $N_1 = 13\,637$ apolar spheres and $N_2 = 718$ dipolar ones in most runs. This corresponds to a mole fraction of $x_2^b = 0.05$ of dipolar spheres in the bulk, roughly the same, at zero field, in the bulk and in the channel. The corresponding (reduced) densities of dipoles and apolar spheres at zero field determined from Monte Carlo (MC) runs are ($\rho_2 = 0.02, \rho_1 = 0.38$) and ($\rho_2 = 0.021, \rho_1 = 0.40$) in the central region of the bulk and the channel, respectively. With the above value of x_2^b, the concentration of the dipolar spheres in the channel saturates for nonzero fields at a lower value than with the smaller $x_2^b = 0.02$ considered in [8,9], but the channel filling with the dipoles is faster.

B. Details of simulations

All MD simulations were conducted using the ESPRESSO package [35,36], modified accordingly to account for the system geometry (Fig. 2) and applied external field [Eq. (3)]. The long-range dipolar forces were evaluated using the dipolar P^{3}M method [37,38]. In this method, the simulation box must be periodic in all three dimensions and therefore the unwanted interaction between periodically replicated systems in the z direction is subtracted using the dipolar layer correction method [39–41]. A time step $\delta t = 0.01\tau_N$ was found sufficient to resolve the composition change in the channel, verified by comparison with a test simulation employing a time step ten times smaller.

Starting from a random distribution of the particles, the system is equilibrated at zero field during at least $\sim 1 \times 10^6$ time steps. To speed up the simulation, a small value of the damping parameter $\gamma^* = 0.046$ is used during the equilibration, in which case the Langevin dynamics acts as a mere thermostat. The field is then turned on and the dynamics is followed by computing at regular time intervals the average number of particles in a channel region of extent a in which the field is nearly uniform (shaded area in Fig. 2), until the concentration saturates. The equilibrium of the system at nonzero field is then monitored during a time $t_{eq} \gtrsim 1 \times 10^6\delta t$. The total length of the field cycles depends of course on t_{eq}, which may vary in the figures shown in the following sections. Therefore, the time elapsed since the field is turned on until the beginning of the equilibrium (when the concentration no longer changes significantly) and similarly at emptying (field off until returning to equilibrium) will be denoted by t_{cycle} and referred to as the field cycle time length. It is thus independent of t_{eq}. As a check of correct equilibration with and without a field, a comparison is made with MC simulations. Finally, the field is turned off and the (possible) emptying of dipoles is monitored similarly until a new equilibrium state is reached.

Depending on the initial state point, one can distinguish between two different scenarios. In the first, after turning the field off, the system returns to its initial state. Molecular dynamics and MC simulations then describe the same equilibrium, as evidenced by the density profiles, for example. For such a state point, the unperturbed system is in the one-phase domain and the field cycle is reversible. In the second scenario the system does not return to its initial state. Such an initial point likely corresponds to a thermodynamic state in which the mixture should be phase separated. Differences are then sometimes found between MC and MD simulations, which explore different, probably metastable, states due to finite system size. The field cycle is then not reversible. We attempt to avoid such state points whose detailed study would require simulating phase equilibria. When this occurs, all coexisting phases would then contribute to the properties of the confined fluid. This might be undesirable for applications that require enough contrast between the response at the filled and empty states.

III. RESULTS

A. Density profiles at equilibrium

After equilibration at $q^* = 0$, the field is switched on and the dipolar spheres begin to fill the channel while simultaneously the apolar spheres leave it, until a new equilibrium is reached. The converse holds when the field is turned off. The results presented here are for a nearly additive mixture;

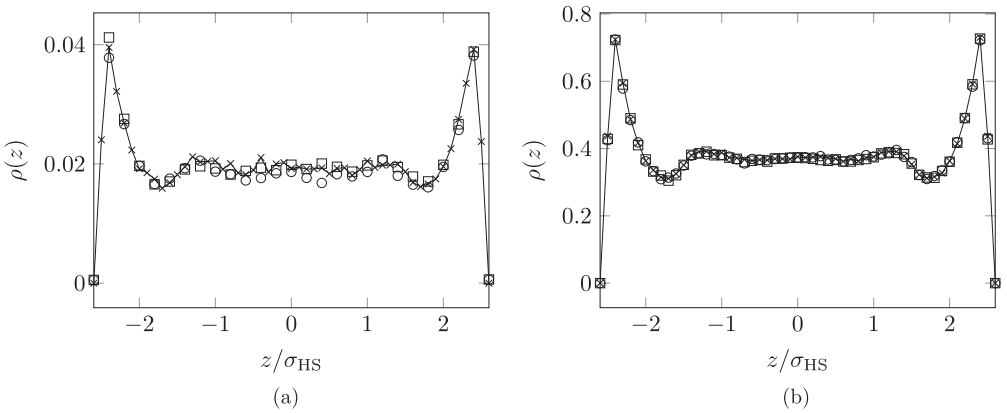

FIG. 4. Density profiles at zero field of (a) dipolar spheres and (b) apolar spheres for MC (crosses) versus MD ($\gamma^* = 0.046$, circles and squares) simulations. Circles and squares correspond to initial ($q^* = 0$) and final ($q^* = 14.3 \rightarrow 0$) states, respectively. Note the difference in the y-axis scale. The lines are guides to the eye.

results for the nonadditive case will be discussed later. A comparison is made with MC simulations to validate the correct equilibrium for the MD simulations.

The density profiles of dipolar and apolar particles inside the channel without an external field ($q^* = 0$ and $q^* = 14.3 \rightarrow 0$) are shown in Fig. 4. The density profiles in Fig. 4(a) are somewhat noisy because of the small number of dipoles in the channel at zero field and the relatively short runs we performed. The figures evidence a normal population in the channel at zero field, essentially the same composition and density of dipolar spheres as in the bulk: $x_2^{\mathrm{p}} \approx 0.05$ and $\rho_2 \approx 0.021$. The return to the initial state after a full cycle $q^* = 0 \rightarrow 14.3 \rightarrow 0$ confirms that indeed the bulk state point is in the one phase domain.

Equilibrium density profiles at $q^* = 14.3$ are shown in Fig. 5. This figure clearly shows a population inversion with respect to the bulk. The density profiles also evidence a preferential population by the dipoles in the region near the walls, a result consistent with previous results for true hard spheres: a progressive wetting by the dipoles [27]. As a normal field favors mixing, the mixture is even more stable at $q^* = 14.3$ than in the absence of the field.

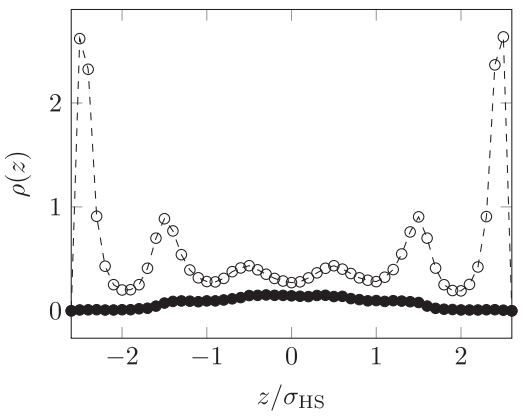

FIG. 5. Plot of the MD ($\gamma^* = 0.046$) density profiles in the channel for $q^* = 14.3$. White and black circles correspond to dipolar and apolar spheres, respectively. The sampling in the x direction was restricted to $x/\sigma_{\mathrm{HS}} \in [-2.5, 2.5]$; cf. Fig. 6.

We conclude this section with a two-dimensional (2D) representation of the total density profile (Fig. 6), with a color modulated by the composition in dipoles. This color map should correspond to the observations in experiments using confocal microscopy. The regions that appear green consist essentially of apolar spheres. This is the case for the entire fluid in Figs. 6(a) and 6(c). After the field is turned on [Fig. 6(b)], the dipoles gather in the central part of the channel, forming an hourglass shape. Similar structuring of dielectric spheres bearing a field-induced dipole are typically analyzed in terms of dielectrophoretic forces [16,19–21,42], following the laws of macroscopic electrostatics. Although in our system permanent dipoles in a field gradient are also drawn to the strong-field region, it is not straightforward to extend the electrostatic argument to our system. This is because of the additional and important role of dipole-dipole interactions as well as the steric interactions with apolar spheres and walls, which favor the preferential adsorption of the dipoles.

B. Dynamics of the composition change

1. Cycling the field reversibly

In this section, we examine the dynamics of population inversion. We first consider a nearly additive mixture at low damping (reduced friction coefficient $\gamma^* = 0.046$). Results for the time evolution of the dipolar spheres mole fraction inside the pore are given in Fig. 7; see also the Supplemental Material for animated snapshots of the filling and emptying [43]. Hereafter, we use the parameters given in Sec. II A to convert the simulation time unit into seconds with the time scale $\tau_{\mathrm{N}} = 2.55 \times 10^{-5} s$. With this scale, one has roughly $t_{\mathrm{cycle}} \sim 0.3$ s in Fig. 7. Several features of the dynamics are notable. (i) The composition of dipolar spheres in the pore x_2^{p} saturates slightly below 0.6. This means that the population inversion is not complete (cf. the results in [9] for an open pore) where the mole fraction of dipoles is $x_2^{\mathrm{p}} \approx 0.98$. This is a consequence of working under canonical conditions and using the nearly additive mixture. The particular combination of parameters used here (x_2^{b} not too small, moderate bulk density) also contributes to give a less marked field-induced variation in x_2^{p} compared to the previous studies in open [9] and

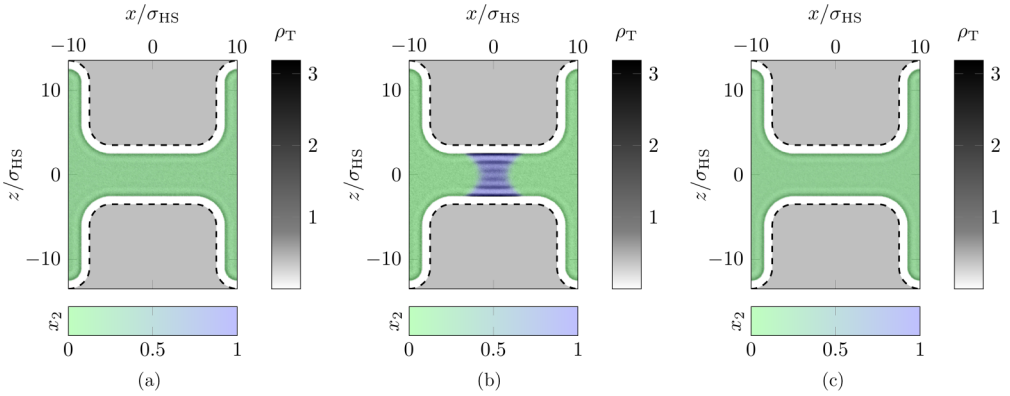

FIG. 6. The 2D density-composition profiles (ρ_T,x_2) from MD simulation with $\gamma^* = 0.046$. The charge densities in the three steps of the field cycle are (a) $q^* = 0$, (b) $q^* = 0 \rightarrow 14.3$, and (c) $q^* = 14.3 \rightarrow 0$.

closed pores [7]. (ii) The filling and emptying dynamics are different. This is understandable considering the contrasting initial conditions: While the dipoles are roughly uniformly distributed throughout the box at zero field, they are mostly concentrated in the channel at nonzero field. (iii) Curiously, just after the field is turned off and emptying begins, x_2^b sharply peaks. This occurs due to an initial decrease in the number of apolar spheres in the channel instead of an increase. This anomalous behavior is most likely due to the sudden expulsion of the dipoles from the channel, which initially also drags a significant number of apolar spheres outside the channel (recall that dipoles that are aligned parallel by the field but not in a head-to-tail configuration repel each other). (iv) After the sharp decrease in x_2^p during emptying, it fluctuates during its relaxation more than prior to filling. These long-lived oscillations, at low damping, are likely a consequence of a large departure from equilibrium of the initial configuration at $q^* = 14.3$ to a channel that has a very small number of dipoles ($N_2 \approx 50$; cf. the number of dipoles in Fig. 10). In Fig. 8, where we used $\gamma^* = 0.46$, which is ten times larger than in Fig. 7, a similar dynamics is observed for both nearly additive and nonadditive mixture. Here t_{cycle} is of course larger, roughly by a factor 5. For different values of γ^*, a nearly linear scaling of the dynamics with γ^* is shown in Fig. 9: Filling curves with increasing values of γ collapse to a single curve when time is scaled by roughly the same factor as γ. A similar observation holds also for the emptying dynamics. We will thus retain the value $t_{cycle} \sim 1.5$ s for $\gamma^* = 0.46$ as the reference for discussing its variation with the physical parameters.

The role of the steric effects is shown in Fig. 10, where we plot the number of dipolar spheres in the pore for the same conditions as in Fig. 8 (green) and for a pure dipolar fluid (red). The filling is naturally faster in the latter case, albeit no population inversion occurs here since the other species is absent. Rather, one gets a smooth field-induced filling of the channel by the dipoles. It was shown in Refs. [8,9] that for a pure dipolar fluid at similar conditions, much larger field magnitudes are required to achieve a sufficient density of dipoles in the pore. Recall that the closer to the bulk instability, the lower the field strength required to observe the PINBI effect. Therefore, unless the field strength is high, the field-induced response will concern mostly the suspending medium, while its content in dipoles is weakly modulated by the field.

The effect of increasing the field strength by a factor of 2 on the filling is shown in Fig. 11. The filling is naturally faster for increasing q, an important observation in relation

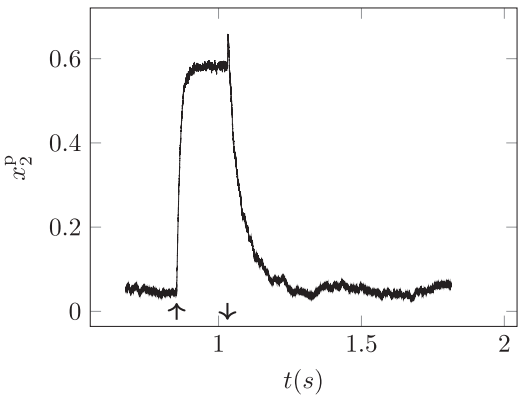

FIG. 7. Filling and emptying dynamics of dipolar spheres inside a channel containing a nearly additive mixture during a cycle $q^* = 0 \rightarrow 14.3 \rightarrow 0$. Here and in the following figures, up and down arrows indicate when the field is turned on and off, respectively. The reduced friction coefficient is $\gamma^* = 0.046$.

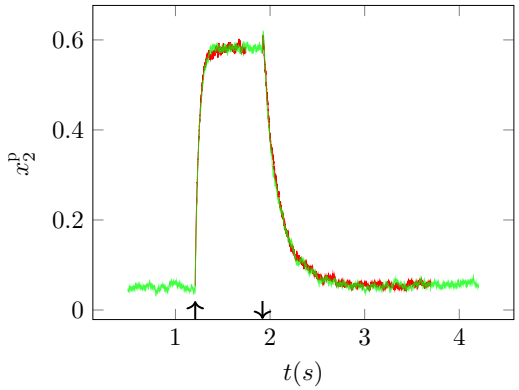

FIG. 8. Filling and emptying of the channel for the cycle $q^* = 0 \rightarrow 14.3 \rightarrow 0$ for nearly additive (red) and nonadditive (green) mixtures. The nearly additive plot was shifted when emptying. The friction coefficient is $\gamma^* = 0.46$.

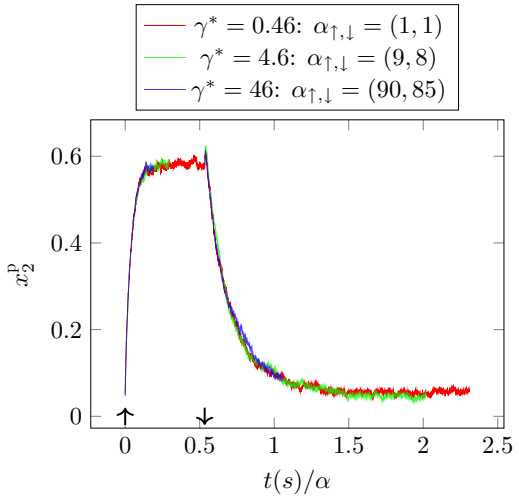

FIG. 9. Filling and emptying versus rescaled time for the cycles $q^* = 14.3 \to 0$ using several dampings. The parameter α with up and down arrows gives the scaling factor for the filling and the emptying, respectively.

to the value of t_{cycle} that one aims at. However, increasing q beyond a certain threshold value has little effect on the filling time and the saturation concentration; the latter even slightly decreases. We attribute this to two competing effects: At increasing field strength, the reduced potential energy of the dipoles inside the pore, which favors filling, also causes an increase of the orientational order of dipoles in the pore and hence increases their lateral repulsion, which is unfavorable to filling. In passing, we note that the decrease of the height of the initial peak at emptying for smaller q is consistent with the interpretation given in the preceding section.

In all the situations discussed above, the field is switched on and off instantaneously. One may of course do this more progressively. We therefore tested also a smooth (sigmoidal) variation of q or a linear one. As expected, the main effect is a smoother filling or emptying, possibly with longer-lived metastable states, for some state points corresponding to a phase separated fluid, which will be discussed in the next section.

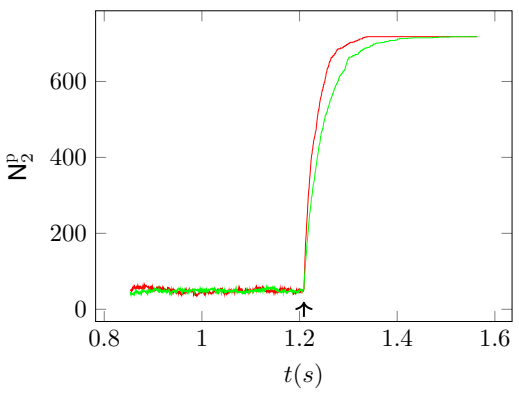

FIG. 10. Filling dynamics for the cycle $q^* = 0 \to 14.3$: pure dipoles (red) vs the nearly additive mixture (green). The friction coefficient $\gamma^* = 0.46$.

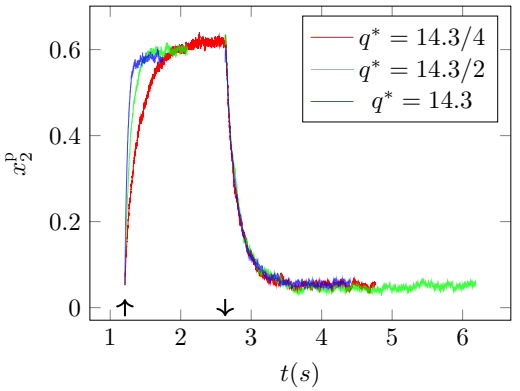

FIG. 11. Filling and emptying for the cycles $q^* = 14.3/4, 14.3/2$, and $14.3 \to 0$ of the nearly additive mixture. The friction coefficient is $\gamma^* = 0.46$.

Our discussion thus far has focused on nearly additive mixtures at state points in which the mixture is in a homogeneous one-phase state, both with and without the applied field. Since the PINBI effect is sensitive to the distance from the bulk instability, it is natural to also study a nonadditive mixture. A full cycle for such a mixture (see Table I), in the same state point we used so far ($\rho^{\mathrm{b}} = 0.40, x_2^{\mathrm{b}} = 0.05$), is shown in Fig. 8. Again, the mixture returns to its initial state. Hence, nonadditivity alone is insufficient, at this state point, to generate a qualitatively different cycle. This is not the case, however, in other state points, as shown in the following section.

2. *Irreversible field cycle*

To illustrate the second kind of behavior, namely, that of irreversible field cycles, we consider a higher $\rho^{\mathrm{b}} = 0.6$ and $x_2^{\mathrm{b}} = 0.1$ for which the nonadditive mixture should be in a two-phase domain at zero field. Starting from a channel nearly empty of dipoles, in a possibly metastable state, the field is switched on and a new equilibrium is reached with almost complete filling $x_2^{\mathrm{p}} \approx 1$. Since a normal field favors mixing, the system is then in a single dipole-rich phase. When the field is switched off, the nonadditive mixture does not return to its initial state in a reasonable time (see Fig. 12); the cycle is irreversible.

In contrast, Fig. 12 also shows that the population inversion in the nearly additive mixture is reversible. This suggests that the nearly additive mixture is at a one-phase state point, though we did not check this by a simulation of the phase equilibrium. For state points corresponding to phase separation, one may view this effect of the field as a means to select one of the coexisting phases, namely, the one rich in dipoles: The initial conditions at zero field with few dipoles should be representative of the dipole-poor phase. For a two-phase state point, after switching on the field and thus favoring a high dipole concentration inside the pore, the system is more likely to remain in this state after turning off the field. Judging from the dipole composition in Fig. 12 after a quite long simulation time, the state that is reached after turning off the field should be close to the actual conjugate phase at zero field.

We plot in Fig. 13 the 2D density-composition maps for the irreversible cycle. When the field is switched on [Fig. 13(b)] the dipoles completely fill the channel and a layered structure

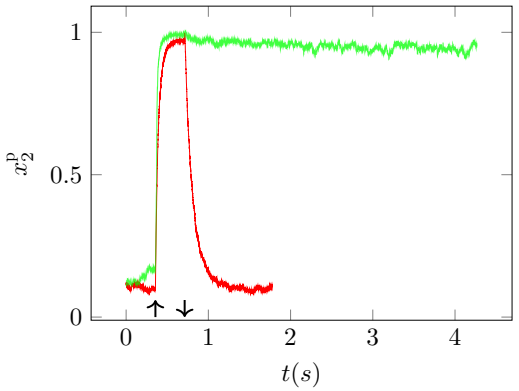

FIG. 12. Cycling the field $q^* = 0 \rightarrow 14.3/2 \rightarrow 0$ for the nearly additive (red) and the nonadditive (green) mixtures. The bulk density and the composition are $\rho^b = 0.6$ and $x_2^b = 0.1$, respectively. The lowest friction coefficient $\gamma^* = 0.046$ was used to speed up the simulation.

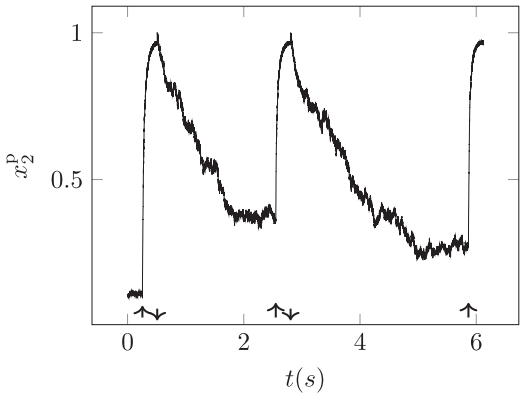

FIG. 14. Reversibly switchable irreversible cycles in the nonadditive mixture. The charge density is $q^* = 0 \rightarrow 14.3/2 \rightarrow 0$. The other parameters are given in the text.

is clearly visible. When the field is switched off [Fig. 13(c)] the layering nearly disappears and the dipole composition in the pore slightly decreases. The boundary between dipolar and apolar spheres remains roughly unchanged, although more diffuse.

As a final illustration of the different behaviors that might be observed with some combinations of the parameters, we show in Fig. 14 a situation in between the two distinct behaviors observed in Fig. 12, for the state point ($\rho^b = 0.52, x_2^b = 0.1$) and $\gamma = 0.046$. For these conditions, the nonadditive mixture does not return to the initial state after cycling the field but to states with higher values $x_2^p \approx 0.35$ and $x_2^p \approx 0.25$, at least in the time window of the figure. That different compositions can be reached after successive extinguishment of the field is a clear indication of nonequilibrium final states. In such situations, we find that a MC run started with the MD configuration obtained after 2×10^4 time steps remains also in states with higher x_2^p compared to the MD simulation, an indication that the Langevin dynamics explore clearly distinct states. A possible cause is that the state is metastable at nonzero field. Interestingly, the full cycle appears reproducible, as other cycles return to the same state at nonzero field. Studying in detail such a situation akin to similar reversibly switchable cycles studied in other contexts (see, for example, [44,45]) is left for future work.

3. Discussion

From the perspective of real experiments, the important point is the time scale of the field-induced transitions. At a given field strength and dipole moment, the relevant parameters are the Newtonian time scale τ_N and the reduced damping parameter $\gamma^* = \gamma\tau_N/m = \tau_N/\tau_R$. One important observation already made above is that the variation of the field cycle time t_{cycle} is roughly linear with γ^*, at least when it is not very small. Here τ_N depends on the particle parameters (size, mass, and interaction strength) and γ on the particle size and solvent viscosity η_s, which is an independent parameter. With $\sigma_{HS} = 1\ \mu$m, $m = 1 \times 10^{-15}$ kg, and $\eta_s = 10^{-3}$ Pa s one gets $\tau_R = 1 \times 10^{-7}$ s. Then, from $B_{WCA}^{(2)} = 2\pi\sigma_{HS}^3/3$ and $\lambda = 0.9$, $\epsilon_{11} = 194 k_B T_a$ gives $\tau_N = 2.55 \times 10^{-5}$ s and hence $\gamma^* = 460$. From the friction coefficient $\gamma = k_B T/D_0$ the diffusion time is $\tau_D \sim 2$ s. The ordering of these time scales is $\tau_R \ll \tau_N \ll \tau_D$, as expected. This means that for colloids one has $\gamma^* \gg 1$.

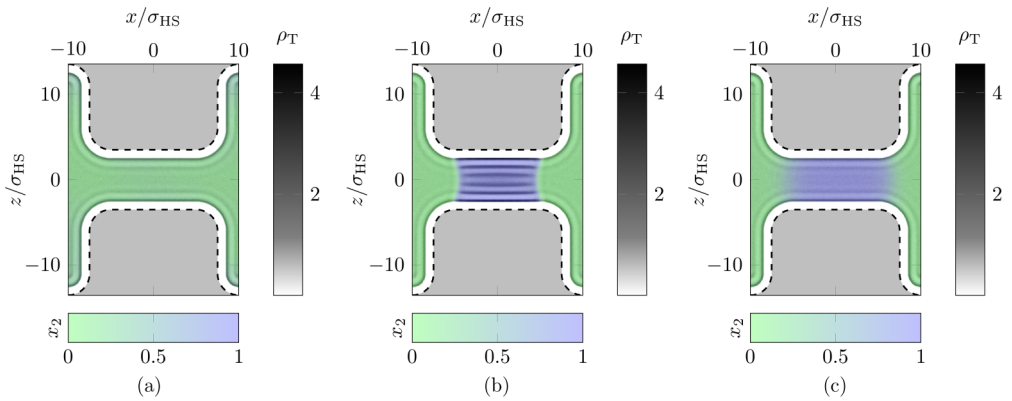

FIG. 13. The 2D density-composition profiles (ρ_T,x_2) from MD simulation with $\gamma^* = 0.046$. The bulk density and composition are $\rho^b = 0.6$ and $x_2^b = 0.1$, respectively. The charge densities in the three steps of the field cycle are (a) $q^* = 0$, (b) $q^* = 0 \rightarrow 14.3/2$, and (c) $q^* = 14.3/2 \rightarrow 0$.

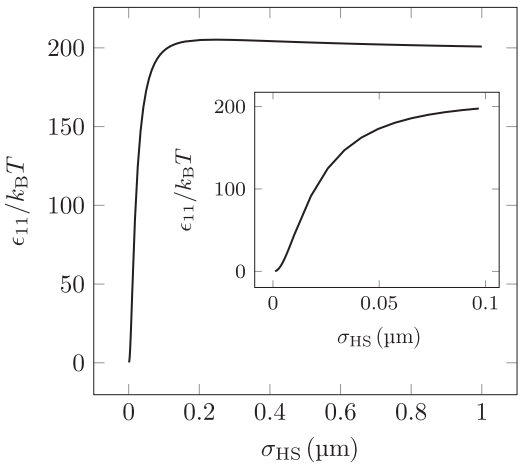

FIG. 15. Interaction strength ϵ_{11}/k_BT of the WCA potential versus colloid diameter σ_{HS}. The inset shows a close-up for small σ_{HS}.

For the value $\gamma^* = 460$ given above, the field cycle shown in Fig. 9 should last approximately $t_{cycle} = 1500$ s, if the other parameters are fixed (in particular τ_N).

To obtain shorter times, one may consider using smaller particles, besides increasing the field, which is inefficient beyond a certain threshold (see Fig. 11). Since m, ϵ_{11}, and γ would also be affected, a model for the structure of the colloidal sphere is necessary. One may nevertheless tentatively estimate the scaling as follows: From its definition and using $\gamma = 3\pi\sigma_{HS}\eta_s$, the reduced friction coefficient scales as $\gamma^* \sim \sigma_{HS}^2/(m\epsilon_{11})^{1/2}$. Since the mass scales as σ_{HS}^3, the variation of γ^* with the particle size is determined by the interaction strength. Insight to the variation of ϵ_{11}/k_BT with the particle size is gained when $B^{(2)}$ is computed for the actual interaction potential ϕ_{SS} between two spheres of Lennard-Jones centers. Although very steep at the scale of σ_{HS}, ϕ_{SS} differs from a pure hard-sphere interaction that yielded a size-independent interaction strength. The scaling of ϵ_{11} with the size can then obtained by solving numerically the equation $B^{(2)}_{WCA} = B^{(2)}_{\phi_{SS}}$ with

$$B^{(2)} = 2\pi \int dr\, r^2 (1 - e^{-u_{ij}(r)/k_BT}) \tag{9}$$

for an interaction potential $u_{ij}(r)$. Here ϕ_{SS} is computed from the model of $1/r^{12}$ centers uniformly distributed in a sphere of diameter σ_{HS} (see [46] for explicit expressions). Ignoring the van der Waals attraction should be reasonable for hard-sphere-like colloids, as in an index-matched dispersion [47]. We used a Hamaker constant $A_H = 5 \times 10^{-20}$ J typical of hydrocarbons [48] and the corresponding diameter $\sigma_{mol} = 0.4$ nm of the molecular species uniformly distributed in the sphere [the WCA diameter was then taken as $\sigma = 0.9(\sigma_{HS} + \sigma_{mol})$, an expression expected to be more realistic for small colloids]. With these conditions, one finds two regimes (see Fig. 15).

(i) For $\sigma_{HS} \gtrsim 0.1$ μm the interaction strength is roughly constant, $\epsilon_{11}/k_BT \sim 200$, because $\phi_{SS}(r)$ is very steep. This would give $\tau_N \sim \sigma_{HS}^{5/2}$, $\gamma^* \sim \sigma_{HS}^{1/2}$, and hence $t_{cycle} \sim \sigma_{HS}^3$. The previous estimation $t_{cycle} = 1500$ s for a size of 1 μm would thus become $t_{cycle} \sim 1.5$ s when using 0.1-μm-sized colloids, i.e., a reduction by a factor 10^3.

(ii) Below 0.1 μm, the interaction strength changes with the size, roughly as σ_{HS}^3 in the range 0.01 μm $\lesssim \sigma_{HS} \lesssim$ 0.1 μm. We thus have $\tau_N \sim \sigma_{HS}$, $\gamma^* \sim 1/\sigma_{HS}$, and hence size-independent time intervals, i.e., $t_{cycle} \lesssim 1.5$ s if all the other variables remain fixed (this cannot strictly hold, for the dipole moment for example). Below 0.01 μm, ϵ_{11} behaves roughly as σ_{HS}^2, giving $\tau_N \sim \sigma_{HS}^{3/2}$ and $\gamma^* \sim 1/\sigma_{HS}^{1/2}$ so that t_{cycle} would decrease linearly with the diameter.

Field cycles even shorter are expected for molecular dimensions. However, one should then keep in mind that our model system assumes flat walls, purely repulsive interactions, etc. On the other hand, our model at high values of γ^* could correspond to colloidal suspensions. Relaxation times are then higher by several orders of magnitude and would however be reliable only for dilute suspensions, since the model lacks the hydrodynamic interactions that exist between macroparticles moving in a molecular fluid. The values $\rho_T \gtrsim 0.4$ used here seem a bit too high to safely neglect hydrodynamic interactions [49–51].

To conclude, realistic estimates of the physical time would require working with a more complete model. It is then necessary to model the system at the appropriate scale and ensure that the reduced parameters used in the computation are consistent with the actual physical parameters. This care for realistic computations is illustrated in some related studies such as that of Edmonds *et al.* [52], who used the same methodology as the one used here to study the forced translocation under an applied voltage of polymers through solid-state nanopores.

IV. CONCLUSION

In summary, we studied the dynamical aspects of the field-induced population change in a confined mixture and confirmed that the field effect can be observed in a realistic geometry. While confirming previous observations pertinent to equilibrium states in infinite pores, the major aspect introduced here is the time evolution towards equilibrium with the switching on or off of the field. We considered the influence of two key parameters: (i) the field strength, showing a nontrivial saturation effect, and (ii) the interaction additivity parameter δ, showing that it can affect the reversibility of the field cycles, opening the possibility to select with the field one of the phases at coexistence. By confirming scaling with the damping parameter of the filling and emptying within Langevin dynamics, it has been possible to extrapolate towards physical times spanning several orders of magnitude. Our results should be helpful in the design of devices based on the dynamical aspects of the composition change [6,15,16]. Finally, depending on the characteristic time scale involved in a specific application, the necessity to improve some aspects of the model to treat molecular or colloidal mixtures has been emphasized.

ACKNOWLEDGMENT

S.S. acknowledges financial support from the European Union's Horizon 2020 program under the Marie Skłodowska-Curie Grant No. 656327.

[1] *Proceedings of the Fourth International Conference on Fundamentals of Adsorption, Kyoto, 1992*, edited by M. Suzuki (Elsevier, Amsterdam, 1993).

[2] Z. Tan and K. E. Gubbins, Selective adsorption of simple mixtures in slit pores: A model of methane-ethane mixtures in carbon, J. Phys. Chem. **96**, 845 (1992).

[3] L. D. Gelb, K. E. Gubbins, R. Radhakrishnan, and M. Sliwinska-Bartkowiak, Phase separation in confined systems, Rep. Prog. Phys. **62**, 1573 (1999).

[4] C. Bechinger, Colloidal suspensions in confined geometries, Curr. Opin. Colloid Interface Sci. **7**, 204 (2002).

[5] A. Yethiraj and A. van Blaaderen, A colloidal model system with an interaction tunable from hard sphere to soft and dipolar, Nature (London) **421**, 513 (2003).

[6] Y. Tsori, F. Tournilhac, and L. Leibler, Demixing in simple fluids induced by electric field gradients, Nature (London) **430**, 544 (2004).

[7] C. Brunet, J. G. Malherbe, and S. Amokrane, Structure of highly confined fluids: Mixture of polar and nonpolar macroparticles in an external field, J. Chem. Phys. **130**, 134908 (2009).

[8] C. Brunet, J. G. Malherbe, and S. Amokrane, Controlling the composition of a confined fluid by an electric field, J. Chem. Phys. **131**, 221103 (2009).

[9] C. Brunet, J. G. Malherbe, and S. Amokrane, Binary mixture adsorbed in a slit pore: Field-induced population inversion near the bulk instability, Phys. Rev. E **82**, 021504 (2010).

[10] Y. Duda, E. Vakarin, and J. Alejandre, Stability and interfacial properties of confined nonadditive hard-sphere binary mixture, J. Colloid Interface Sci. **258**, 10 (2003).

[11] F. Jiménez-Ángeles, Y. Duda, G. Odriozola, and M. Lozada-Cassou, Population inversion of a nahs mixture adsorbed into a cylindrical pore, J. Phys. Chem. C **112**, 18028 (2008).

[12] S.-C. Kim, S.-H. Suh, and B.-S. Seong, Population inversion of confined symmetric nonadditive hard-sphere mixtures, J. Korean Phys. Soc. **54**, 660 (2009).

[13] E.-Y. Kim, S.-C. Kim, and B.-S. Seong, Nonadditive penetrable mixtures in nanopores: Surface-induced population inversion, J. Phys. Chem. B **116**, 3180 (2012).

[14] J. Jordanovic and S. H. L. Klapp, Field-Induced Layer Formation in Dipolar Nanofilms, Phys. Rev. Lett. **101**, 038302 (2008).

[15] M. T. Sullivan, K. Zhao, A. D. Hollingsworth, R. H. Austin, W. B. Russel, and P. M. Chaikin, An Electric Bottle for Colloids, Phys. Rev. Lett. **96**, 015703 (2006).

[16] M. E. Leunissen, M. T. Sullivan, P. M. Chaikin, and A. van Blaaderen, Concentrating colloids with electric field gradients. I. particle transport and growth mechanism of hard-sphere-like crystals in an electric bottle, J. Chem. Phys. **128**, 164508 (2008).

[17] H. Löwen, Twenty years of confined colloids: from confinement-induced freezing to giant breathing, J. Phys.: Condens. Matter **21**, 474203 (2009).

[18] J. Richardi, M. P. Pileni, and J. J. Weis, Self-organization of confined dipolar particles in a parallel field, J. Chem. Phys. **130**, 124515 (2009).

[19] G. Marcus, S. Samin, and Y. Tsori, Phase-separation transition in liquid mixtures near curved charged objects, J. Chem. Phys. **129**, 061101 (2008).

[20] S. Samin and Y. Tsori, Stability of binary mixtures in electric field gradients, J. Chem. Phys. **131**, 194102 (2009).

[21] S. Samin and Y. Tsori, Vapor-liquid equilibrium in electric field gradients, J. Phys. Chem. B **115**, 75 (2011).

[22] S. Samin, Y. Tsori, and C. Holm, Vapor-liquid coexistence of the Stockmayer fluid in nonuniform external fields, Phys. Rev. E **87**, 052128 (2013).

[23] H. Löwen, Introduction to colloidal dispersions in external fields, Eur. Phys. J. Spec. Top. **222**, 2727 (2013).

[24] R. Roth and D. Gillespie, Physics of Size Selectivity, Phys. Rev. Lett. **95**, 247801 (2005).

[25] R. Roth, M. Rauscher, and A. J. Archer, Selectivity in binary fluid mixtures: Static and dynamical properties, Phys. Rev. E **80**, 021409 (2009).

[26] C. Brunet, J. G. Malherbe, and S. Amokrane, Demixing and field-induced population inversion in a mixture of neutral and dipolar-hard spheres confined in a slit pore, Mol. Phys **110**, 1161 (2012).

[27] S. Chung, J. G. Malherbe, and S. Amokrane, Effect of an external field on the structure and the phase transitions of a confined mixture of neutral and dipolar hard spheres, Mol. Phys. **113**, 3216 (2015).

[28] H. Schmidle and S. H. L. Klapp, Phase transitions of two-dimensional dipolar fluids in external fields, J. Chem. Phys. **134**, 114903 (2011).

[29] N. Li, H. D. Newman, M. Valera, I. Saika-Voivod, and A. Yethiraj, Colloids with a tunable dipolar interaction: Equations of state and order parameters viaconfocal microscopy, Soft Matter **6**, 876 (2010).

[30] B. Peng, E. van der Wee, A. Imhof, and A. van Blaaderen, Synthesis of monodisperse, highly cross-linked, fluorescent PMMA particles by dispersion polymerization, Langmuir **28**, 6776 (2012).

[31] J. D. Weeks, Role of repulsive forces in determining the equilibrium structure of simple liquids, J. Chem. Phys. **54**, 5237 (1971).

[32] M. Rovere and G. Pastore, Fluid-fluid phase separation in binary mixtures of asymmetric non-additive hard spheres, J. Phys.: Condens. Matter **6**, A163 (1994).

[33] P. Hopkins and M. Schmidt, Binary non-additive hard sphere mixtures: Fluid demixing, asymptotic decay of correlations and free fluid interfaces, J. Phys. Condens. Matt. **22**, 325108 (2010).

[34] C. Brunet, J. G. Malherbe, and S. Amokrane, Monte Carlo simulation of confined fluids of polarizable particles: An efficient iterative treatment of the local field in slab geometry using Ewald summation, Mol. Phys **108**, 1773 (2010).

[35] H.-J. Limbach, A. Arnold, B. A. Mann, and C. Holm, ESPResSo—An extensible simulation package for research on soft matter systems, Comput. Phys. Commun. **174**, 704 (2006).

[36] A. Arnold, O. Lenz, S. Kesselheim, R. Weeber, F. Fahrenberger, D. Roehm, P. Košovan, and C. Holm, in *Meshfree Methods for Partial Differential Equations VI*, edited by M. Griebel and M. A. Schweitzer, Lecture Notes in Computational Science and Engineering Vol. 89 (Springer, Berlin, 2013), pp. 1–23.

[37] J. J. Cerdà, V. Ballenegger, O. Lenz, and C. Holm, P^3M algorithm for dipolar interactions, J. Chem. Phys. **129**, 234104 (2008).

[38] J. J. Cerdà, V. Ballenegger, and C. Holm, Particle-particle particle-mesh method for dipolar interactions: On error estimates and efficiency of schemes with analytical differentiation and mesh interlacing, J. Chem. Phys. **135**, 184110 (2011).

[39] A. Arnold, J. de Joannis, and C. Holm, Electrostatics in periodic slab geometries. I, J. Chem. Phys. **117**, 2496 (2002).

[40] J. de Joannis, A. Arnold, and C. Holm, Electrostatics in periodic slab geometries. II, J. Chem. Phys. **117**, 2503 (2002).

[41] A. Bródka, Ewald summation method with electrostatic layer correction for interactions of point dipoles in slab geometry, Chem. Phys. Lett. **400**, 62 (2004).

[42] Y. Tsori, Colloquium: Phase transitions in polymers and liquids in electric fields, Rev. Mod. Phys. **81**, 1471 (2009).

[43] See Supplemental Material at http://link.aps.org/supplemental/10.1103/PhysRevE.95.022605 for animated filling and emptying of the pore.

[44] H. Gu, L. Bi, Y. Fu, N. Wang, S. Liu, and Z. Tang, Multistate electrically controlled photoluminescence switching, Chem. Sci. **4**, 4371 (2013).

[45] M. Liebi, S. Kuster, J. Kohlbrecher, T. Ishikawa, P. Fischer, P. Walde, and E. J. Windhab, Magnetically enhanced bicelles delivering switchable anisotropy in optical gels, ACS Appl. Mater. Interfaces **6**, 1100 (2014).

[46] D. Henderson, D.-M. Duh, X. Chu, and D. Wasan, An expression for the dispersion force between colloidal particles, J. Colloid Interface Sci. **185**, 265 (1997).

[47] S.-E. Phan, W. B. Russel, Z. Cheng, J. Zhu, P. M. Chaikin, J. H. Dunsmuir, and R. H. Ottewill, Phase transition, equation of state, and limiting shear viscosities of hard sphere dispersions, Phys. Rev. E **54**, 6633 (1996).

[48] J. Israelachvili, *Intermolecular and Surface Forces*, 3rd ed. (Academic, New York, 2011).

[49] H. Löwen, Colloidal dispersions in external fields: recent developments, J. Phys.: Condens. Matter **20**, 404201 (2008).

[50] K. Grass and C. Holm, Polyelectrolytes in electric fields: Measuring the dynamical effective charge and effective friction, Soft Matter **5**, 2079 (2009).

[51] M. Heinen, A. J. Banchio, and G. Nägele, Short-time rheology and diffusion in suspensions of Yukawa-type colloidal particles, J. Chem. Phys. **135**, 154504 (2011).

[52] C. M. Edmonds, Y. C. Hudiono, A. G. Ahmadi, P. J. Hesketh, and S. Nair, Polymer translocation in solid-state nanopores: Dependence of scaling behavior on pore dimensions and applied voltage, J. Chem. Phys. **136**, 065105 (2012).